Max-Planck-Institut
für Mathematik
in den Naturwissenschaften
Leipzig

A highly accurate full subtraction approach for dipole modelling in EEG source analysis using the finite element method

by

Florian Drechsler, Carsten H. Wolters, Thomas Dierkes, Hang Si, and Lars Grasedyck

Preprint no.: 95 2007

A highly accurate full subtraction approach for dipole modelling in EEG source analysis using the finite element method

F. Drechsler[1], C. H. Wolters[2,*], T. Dierkes[2], H. Si[3], L. Grasedyck[1]

(1) Max-Planck-Institut für Mathematik in den Naturwissenschaften, Leipzig, Germany
(2) Institut für Biomagnetismus und Biosignalanalyse, Westfälische Wilhelms-Universität Münster, Münster, Germany
(3) Weierstraß-Institut für Angewandte Analysis und Stochastik, Berlin, Germany.

Abstract

A mathematical dipole is widely used as a model for the primary current source in electroencephalography (EEG) source analysis. In the governing Poisson-type differential equation, the dipole leads to a singularity on the right-hand side, which has to be treated specifically. In this paper, we will present a full subtraction approach where the total potential is divided into a singularity and a correction potential. The singularity potential is due to a dipole in an infinite region of homogeneous conductivity. The correction potential is computed using the finite element (FE) method. Special care is taken to appropriately evaluate the right-hand side integral with the objective of achieving highest possible convergence order for linear basis functions. Our new approach allows the construction of transfer matrices for fast computation of the inverse problem for volume conductors with arbitrary local and remote conductivity anisotropy. A constrained Delaunay tetrahedralisation (CDT) approach is used for the generation of high-quality FE meshes. We validate the new approach in a four-layer sphere model with anisotropic skull compartment. For radial and tangential sources with eccentricities up to 1mm below the cerebrospinal fluid compartment, we achieve a maximal relative error of 0.71% in a tetrahedra model with 360K nodes which is not locally refined around the source singularity. The combination of the full subtraction approach with the high quality CDT meshes leads to accuracies that, to the best of the authors knowledge, have not yet been presented before.

Key words: source reconstruction, electroencephalography, finite element method, dipole, full subtraction approach, constrained Delaunay tetrahedralisation, validation in four-layer sphere models, projected subtraction approach, transfer matrices

1 Introduction

Inverse methods are used to reconstruct current sources in the human brain by means of electroencephalography (EEG) or magnetoencephalography (MEG) measurements of, e.g., event related fields or epileptic seizures [15,18,30]. A critical component of the inverse neural source reconstruction is the solution of the forward problem [32], i.e., the simulation of the fields at the head surface for a known primary current source in the brain. Because of the availability of quasi-analytical forward problem solution formulas, the head volume conductor is still often represented by a multi-layer sphere model [6]. However, this model is just a rough approximation to the reality, so that numerical approximation methods are more and more frequently used such as the boundary element method (BEM) [**?**], the finite volume method (FVM) [16], the finite difference method (FDM) [11] or the finite element method (FEM) [3,1,29,13,23,33]. We will focus on the FEM because of its enormous ability and accuracy in modelling the forward problem in geometrically complicated inhomogeneous and anisotropic volume conductors, as will be presented in this paper.

It is shown in [22,7,17] that the mathematical dipole is an adequate model to represent the primary current which is caused by a synchronous activity of tens of thousands of densely packed apical dendrites of large pyramidal cells oriented in parallel in the human cortex. The dipole model is thus considered to be the "atomic" structure of the primary current density distribution that has to be reconstructed within the inverse problem. Hence, one of the key questions for all 3D forward modelling techniques is the appropriate modelling of the potential singularity introduced into the differential equation by means of the mathematical dipole.

Direct potential approaches [38,5] approximate the dipole moment through optimally distributed monopolar sources and sinks on neighbouring FE nodes of the source location. This approach leads to finite distances between the poles that seem reasonable as it performs well in validation studies [5,35]. However, direct approaches are strongly mesh-dependent and bear the risk that monopoles are introduced into compartments with different conductivities. Another disadvantage of direct approaches is the absence of a well-understood mathematical theory, especially the interplay with tissue anisotropy is not yet sufficiently examined. In recent comparison studies of different direct meth-

* Corresponding author. Institut für Biomagnetismus und Biosignalanalyse, Westfälische Wilhelms-Universität Münster, Malmedyweg 15, 48149 Münster, Germany, Tel.: +49/(0)251-83-56904, Fax: +49/(0)251-83-56874, http://biomag.uni-muenster.de

Email address: fdr@mis.mpg.de,carsten.wolters@uni-muenster.de, thomas.dierkes@uni-muenster.de,si@wias-berlin.de,lgr@mis.mpg.de (F. Drechsler[1], C. H. Wolters[2,*], T. Dierkes[2], H. Si[3], L. Grasedyck[1]).

ods with the subtraction approach [1,23], it is concluded that the overall best performance is achieved using the latter method.

A subtraction approach for the modelling of a mathematical dipole in FE-based source analysis is widely suggested [3,1,29,13,23,33]. All proposed approaches have in common that the total potential is divided into an analytically known singularity potential and a singularity-free correction potential which can then be approximated numerically using an FE approach. In [33], we give a theoretical insight into the subtraction approach. A proof is given for existence and uniqueness of the weak solution in the function space of zero-mean potential functions and convergence properties of the FE-approach to the correction potential are stated. In this article, a *projected subtraction method* is proposed where the singularity potential is projected in the FE space. This approach is shown to perform well in a three-compartment (skin, skull, brain) sphere model with anisotropic skull compartment provided that the so-called *source eccentricity* is limited to 95%. The eccentricity is generally defined as the percent ratio of the distance between the source location and the model midpoint divided by the radius of the inner sphere. When considering a three-shell model, 95% eccentricity seems reasonable because the dipoles that are located in the cortex will have an eccentricity even lower than 92% as reported in [13].

However, the three-compartment model of the head ignores the cerebrospinal fluid (CSF) compartment between the cortex and the skull. The CSF has a much higher conductivity than the brain compartment [2]. Additionally. it is shown to have a significant influence on the forward problem [21,31]. In four-compartment models, this layer is taken into account, but source eccentricity then has to be determined with regard to the inner CSF surface, i.e., the most eccentric sources are only 1 or 2mm apart from the next conductivity discontinuity. Therefore, eccentricities of more than 98% have to be examined. It is well-known (and in [33], a theoretical reasoning is given for this fact), that with increasing eccentricity, the numerical accuracy in sphere model validations decreases [3,29,13,33]. This is not only the case for the subtraction approach, but also for the direct approach in FE modelling [38,5] and in BE modelling (see, e.g., [**?**]). In [3,29,13], coarse tetrahedral meshes are considered yielding unacceptably large numerical errors already at eccentricities above 90%. In [3,29], local mesh refinement around the source is used to achieve better results. However, with regard to the inverse problem, the setup of source-location dependent locally refined meshes is difficult to implement and time-consuming to compute and thus might not be practicable for an inverse source analysis.

In this paper, we propose a so-called *full subtraction approach* which appropriately evaluates the right-hand side integral for the correction potential with the objective of achieving highest possible convergence order for linear basis functions. Our new approach does not need local mesh refinement around the

source. As we will show, it therefore allows the construction of transfer matrices for fast computation of the inverse problem for volume conductors with arbitrary local (at the source position, i.e., grey matter) and remote (with a minimal distance to the source position, i.e., white matter) conductivity anisotropy. The transfer matrices are introduced for the projected subtraction method in [37,33], but those developments are still limited to the modelling of only remote anisotropy. A constrained Delaunay tetrahedralisation (CDT) approach is used for the generation of high-quality FE meshes, while former studies are limited to ordinary Delaunay tetrahedralisation [33]. We validate the new approach in a four-layer sphere model with anisotropic skull compartment and sources up to 1mm below the CSF compartment. We compare the accuracy of our new method with the projected subtraction approach from [33] and the literature. It will be shown that the combination of the full subtraction approach with the CDT-FE meshes leads to very high accuracies.

2 The Continuous Forward Problem

The mathematical model for the numerical simulation of electric and magnetic fields in the human head is based on the quasistatic approximation of Maxwell's equations. A linearisation of these equations leads to the following forward problem in source analysis [20,22]:

Assumption 1 *Let $\sigma : \mathbb{R}^3 \to \mathbb{R}^{3\times 3}$ be a mapping such that $\sigma(x)$ is a symmetric positive definite 3×3 matrix (the electric conductivity depending on x), and let $\Omega \subset \mathbb{R}^3$ be a bounded polygonal domain (the head). For each $y \in \Omega$ a vector $M(y) \in \mathbb{R}^3$ (the current dipolar moment) is given.*

Notation 2 *(1) We denote the divergence of a function $f : \Omega \to \mathbb{R}^3$ by*

$$\mathrm{div} f(x) := \sum_{j=1}^{3} \partial_j f(x).$$

(2) The gradient of a function $f : \Omega \to \mathbb{R}$ is the vector

$$\nabla f(x) := (\partial_1 f(x), \partial_2 f(x), \partial_3 f(x)).$$

(3) By $n(x)$ we denote the outer unit normal of Ω at the point $x \in \partial\Omega$.

Definition 3 (The continuous forward problem) *The forward problem in source analysis is to find for each primary current density function*

$$f = f^y, \quad f^y(x) = \mathrm{div} M(y)\delta(x-y), \qquad y \in Y \subset \Omega, \;\; M(y) \in \mathbb{R}^3, \qquad (1)$$

a solution for the electric potential u (in an appropriate space) such that

$$\begin{aligned} \operatorname{div} \sigma(x)\, \nabla u(x) &= f(x) \quad \text{for a.e. } x \in \Omega, \\ \langle \sigma(x) \nabla u(x), n(x) \rangle &= 0 \quad \text{for a.e. } x \in \partial\Omega, \\ \int_\Omega u(x) dx &= 0. \end{aligned} \tag{2}$$

Here δ denotes the Dirac delta distribution and $\langle \cdot, \cdot \rangle$ the inner product.

In order to understand the difficulties of a discretisation of the forward problem we consider a simple example where the solution is known analytically.

Example 4 *Let $y \in \Omega$. For the case $\Omega = \mathbb{R}^3$ (unbounded!) and $\sigma(x) \equiv \sigma(y)$ for all $x \in \Omega$, the solution $u^{\infty,y}$ for the right-hand side f^y of (2) is*

$$u^{\infty,y}(x) := \frac{1}{4\pi\sqrt{\det \sigma(y)}} \frac{\langle M(y), \sigma(y)^{-1}(x-y) \rangle}{\langle \sigma(y)^{-1}(x-y), x-y \rangle^{3/2}}. \tag{3}$$

At infinity ($x \to \infty$) it fulfills the Neumann boundary conditions. The singularity of $u^{\infty,y}$ at $x = y$ is of order 2, so that $u^{\infty,y}$ does not belong to $H^1(\Omega)$ (refer, e.g., to [4] for a definition of the function spaces), not even $L^2(\Omega)$. In order to resolve the singularity in the discretisation, one would have to include special singular basis functions or use a locally refined grid.

In the following, we will derive a continuous formulation where the singularity in the right-hand side is removed so that standard discretisation techniques are applicable.

3 Full Subtraction Approach and Finite Element Discretisation

In order to apply a finite element discretisation, we have to reformulate the problem, because neither the right-hand side f nor the solution u allow for a good approximation by standard finite elements. Moreover, the variational formulation would require an integration by parts (Gauß integral theorem, resp. Green's identity), which might not be applicable for general functions like u that are not in $H^1(\Omega)$.

Definition 5 (Continuous subtraction forward problem) *Let $u^{\infty,y}$ denote the solution defined in (3). The subtraction forward problem is to find for each*

$$f = f^y, \quad f^y(x) = \operatorname{div} M(y) \delta(x-y),$$

a solution $u^{\mathrm{corr,y}}$ (in an appropriate space) such that

$$
\begin{aligned}
\text{div } \sigma(x)\, \nabla(u^{\text{corr,y}}(x) + u^{\infty,y}(x)) &= f(x) \quad \textit{for a.e. } x \in \Omega, \\
\langle \sigma(x) \nabla(u^{\text{corr,y}}(x) + u^{\infty,y}(x)), n(x) \rangle &= 0 \quad \textit{for a.e. } x \in \partial\Omega, \\
\int_\Omega (u^{\text{corr,y}}(x) + u^{\infty,y}(x)) dx &= 0.
\end{aligned} \tag{4}
$$

Equation (4) can be written in the form

$$
\begin{aligned}
\text{div } \sigma(x)\, \nabla u^{\text{corr,y}}(x) &= \text{div } (\sigma(y) - \sigma(x))\, \nabla u^{\infty,y}(x) \quad \text{for a.e. } x \in \Omega, \\
\langle \sigma(x) \nabla u^{\text{corr,y}}(x), n(x) \rangle &= -\langle \sigma(x) \nabla u^{\infty,y}(x), n(x) \rangle \quad \text{for a.e. } x \in \partial\Omega, \\
\int_\Omega u^{\text{corr,y}}(x) dx &= -\int_\Omega u^{\infty,y}(x) dx.
\end{aligned} \tag{5}
$$

In order to remove the singularities in the right-hand side of (5), we need the assumption that the difference $\sigma(y) - \sigma(x)$ vanishes in a ball around y.

Assumption 6 *Let $\epsilon > 0$ s.t. for every $y \in Y$, the tensor $\sigma(x)$ is constant in a small ball*

$$\Omega_\epsilon^y := \{x \in \Omega \mid \|x - y\|_2 < \epsilon\} \subset \Omega$$

around y.

Lemma 7 *Using the Assumption 6, the right-hand side*

$$\text{div}(\sigma(y) - \sigma(x))\, \nabla u^{\infty,y}(x)$$

in (5) belongs to $L^2(\Omega)$.

Proof: Let $\overline{u}^{\infty,y}$ denote a smooth extension of $u^{\infty,y}$ for all $x \in \Omega \setminus \Omega_\epsilon^y$. Then,

$$(\sigma(y) - \sigma(x)) \nabla \overline{u}^{\infty,y}(x) = (\sigma(y) - \sigma(x)) \nabla u^{\infty,y}(x) \quad \forall x \in \Omega \setminus \Omega_\epsilon^y$$

holds. The function $\overline{u}^{\infty,y}$ is smooth in $\Omega \setminus \Omega_\epsilon^y$ so that $div(\sigma(y) - \sigma(x)) \nabla \overline{u}^{\infty,y}$ is smooth in $\Omega \setminus \Omega_\epsilon^y$. Hence $u^{\infty,y}$ is smooth in $\Omega \setminus \Omega_\epsilon^y$. With the assumption 6, it is

$$(\sigma(y) - \sigma(x)) \nabla u^{\infty}(x) = 0 \quad \forall x \in \Omega_\epsilon^y.$$

Therefore $u^{\infty,y}$ is in $L^2(\Omega)$. ■

Assumption 8 *Let $V \subset H^1(\Omega)$ be an infinite space and let $V_N \subset V$ be an N-dimensional subspace of V.*

The role of V_N is that of a finite element space, e.g. piecewise polynomials up to a certain degree. The space V might, due to higher regularity assumptions, be $H^{1+\varepsilon}(\Omega)$ with $\varepsilon \in]0,1[$.

Now we can apply the Gauß integral theorem

$$\begin{aligned}\int_\Omega v(x)\mathrm{div}\sigma(x)\nabla u(x)dx = &-\int_\Omega \langle \nabla v(x), \sigma(x)\nabla u(x)\rangle dx \\ &+\int_{\partial\Omega} v(x)\langle n(x), \sigma(x)\nabla u(x)\rangle dx\end{aligned}$$

and arrive at the variational formulation that is suitable for a finite element discretisation.

Definition 9 (Analytical forward problem) *For an arbitrary mapping $\alpha : \Omega \to \mathbb{R}^{3\times 3}$ we define the bilinear form*

$$a_\alpha : V \times V \to \mathbb{R}, \quad a_\alpha(u,v) := \int_\Omega \langle \alpha(x)\nabla u(x), \nabla v(x)\rangle dx.$$

The analytical forward problem is to find $u^{corr,y} \in V$ s.t.

$$\begin{aligned}\forall v \in V: \quad a_\sigma(u^{corr,y}, v) &= a_{\sigma(y)-\sigma}(u^{\infty,y}, v) - \int_{\partial\Omega} v(x)\langle n(x), \sigma(y)\nabla u^{\infty,y}(x)\rangle dx, \\ \int_\Omega u^{corr,y}(x)dx &= -\int_\Omega u^{\infty,y}(x)dx.\end{aligned}$$

In [33, section 3.5], it is shown that a unique solution of the analytical forward problem exists and the solution $u^{corr,y}$ belongs to $H^1(\Omega)$.

Definition 10 (Finite element forward problem) *The finite element forward problem is to find $u_N \in V_N$ s.t.*

$$\begin{aligned}&\forall v \in V_N: \\ &a_\sigma(u_N, v) = a_{\sigma(y)-\sigma}(u^{\infty,y}, v) - \int_{\partial\Omega} v(x)\langle n(x), \sigma(y)\nabla u^{\infty,y}(x)\rangle dx, \\ &\int_\Omega u_N(x)dx = -\int_\Omega u^{\infty,y}(x)dx.\end{aligned}$$

Let $\tau = \{\tau_1, \ldots, \tau_T\}$ be a triangulation of the polygonal domain Ω into tetrahedra τ_i. For the finite element space V_N we use standard conforming linear elements, i.e. $V_N = \{v \in V \mid v|_{\tau_i} \text{ affine } \forall i = 1, \ldots, T\}$. Let $\operatorname{span}\{\varphi_i \mid i \in \mathcal{I}\}$ denote the standard Lagrange basis of V_N using local basis functions φ_i, $i \in \mathcal{I}, \#\mathcal{I} = N$. By ξ_i we denote the Lagrange point of the FE basis function φ_i.

The linear system to be solved is

$$Ku = b, \tag{6}$$

where the entries of the stiffness matrix K and right-hand side b are

$$K_{i,j} := a_\sigma(\varphi_j, \varphi_i),$$

$$b_i := \int_\Omega \langle (\sigma(y) - \sigma(x)) \nabla u^{\infty,y}(x), \nabla \varphi_i(x) \rangle dx \tag{7}$$

$$- \int_{\partial\Omega} \varphi_i(x) \langle n(x), \sigma(y) \nabla u^{\infty,y}(x) \rangle dx. \tag{8}$$

The discrete solution is

$$u_N(x) = \sum_{i \in \mathcal{I}} u_i \varphi_i(x).$$

The gradient of $u^{\infty,y}$ is

$$\begin{aligned} \nabla u^{\infty,y}(x) = & \frac{1}{4\pi\sqrt{\det \sigma(y)}} \cdot \frac{\sigma(y)^{-1} M(y)}{\langle \sigma(y)^{-1}(x-y), x-y \rangle^{3/2}} \\ & - \frac{1}{4\pi\sqrt{\det \sigma(y)}} \cdot \frac{3\langle M(y), \sigma(y)^{-1}(x-y) \rangle \sigma(y)^{-1}(x-y)}{\langle \sigma(y)^{-1}(x-y), x-y \rangle^{5/2}}. \end{aligned}$$

Remark 11 *(1) The term $\nabla\varphi_i$ is constant for linear elements. Thus, entries of K can be computed easily.*

(2) The entries of the right-hand side need to be accurate enough in order to preserve the finite element convergence. Since we project the correction potential into the space V_N of piecewise linear elements, it is sufficient to have a perturbation of size $\mathcal{O}(h^2)$ which is achieved by a second order accurate quadrature formula. In the numerics section we will verify that this order is necessary and sufficient to produce a negligible quadrature error.

(3) We assemble the first term of b_i element-wise where each element contributes to $\mathcal{O}(1)$ entries. For $x \to y$ the integral even vanishes, cf. Assumption 6. The second term involves the normal vector and the basis function itself. Thus, we need a quadrature formula that resolves $\nabla u^{\infty,y}$ at the boundary (where it is very smooth) and that is accurate for linear functions. Again, a second order quadrature formula for the surface triangles is necessary and sufficient.

In [33], a projected subtraction approach is presented where the function $u^{\infty,y}$ is projected in the finite element space V_N by

$$u^{\infty}(x) \approx u_N^{\infty}(x) = \sum_{i=1}^{N} \varphi_i(x) u_i^{\infty}, \quad u_i^{\infty} = u^{\infty}(\xi_i). \tag{9}$$

Introducing the coefficient vector $u_\infty := (u_1^\infty, \ldots, u_N^\infty)$, the equation system

$$Ku = -K^{corr} u_\infty - S u_\infty,$$

is obtained where the matrices are defined by

$$K_{i,j}^{corr} := -\int_{\Omega} \langle (\sigma(y) - \sigma(x)) \nabla \varphi_i(x), \nabla \varphi_j(x) \rangle dx \tag{10}$$

and

$$S_{i,j} := \int_{\partial\Omega} \langle \sigma(y) \nabla \varphi_j(x), n(x) \rangle \varphi_i(x) dx. \tag{11}$$

The drawback of the projected subtraction approach to compute the correction potential is the additional approximation error by (9). We will see in the numerical validation section that the presented full subtraction approach in which u^∞ is not approximated in the space V_N, has a much higher degree of accuracy.

4 Transfer matrix

The forward problem in EEG and MEG source analysis has to be solved for many right-hand sides $f = f^y$, $y \in Y$ (most often several thousands). In this case, the following assumption is necessary for an efficient computation of all solutions.

Assumption 12 *We demand that the FE mesh is the same for all right-hand*

sides $f = f^y$, i.e., we want to avoid local mesh refinement with regard to a specific source location.

However, the full solution vector is not required for all right-hand sides. Instead, only a linear transform of the function u,

$$Au \in \mathbb{R}^m, \qquad m \ll N, \quad A : V \to \mathbb{R}^m,$$

is of interest with m being the number of measurement sensors. In this case, one can precompute the so-called *transfer matrix*

$$B := \hat{A}K^{-1} \in \mathbb{R}^{m \times N}$$

where $\hat{A}$ is the matrix representation of the linear mapping A restricted to the finite dimensional space V_N in the basis $\{\varphi_i \mid i \in \mathcal{I}\}$ [37] [1]. In case of the EEG, $\hat{A}$ is either a restriction or a surface interpolation of the potential vector to those FE nodes which represent the EEG electrodes. In case of the MEG, $\hat{A}$ is the secondary flux integration matrix [37].

The full subtraction method EEG forward solution is thus obtained by

$$Au \approx A(u_N + u^{\infty,y}) = \hat{A}K^{-1}b + \hat{A}u^{\infty,y} = Bb + \hat{A}u^{\infty,y},$$

a matrix-vector multiplication with the $m \times N$ transfer matrix B. The MEG forward solution can exploit the precomputed MEG transfer matrix in a very similar fashion for the secondary magnetic flux parts [37]. The setup of the transfer matrix B requires m times the solution of the $N \times N$ system K. Using an optimal method, e.g., multigrid, this can be done in $\mathcal{O}(m \cdot N)$ [10, Theorem 10.4.2]. The term $\hat{A}u^{\infty,y}$ can be computed easily because the solution $u^{\infty,y}$ is given analytically and it is smooth at the boundary where the support of $\hat{A}$ typically lies.

The projected subtraction approach [33] leads to the transfer matrix

$$\hat{A}K^{-1}(-K^{corr} - S).$$

This approach is only useful, if all right-hand sides f^y have the same conductivity at all possible cortical source positions. This means that for the projected subtraction approach,

$$\sigma(y) = \sigma_c, \sigma_c \in \mathbb{R}^{3\times 3}, \sigma_c \text{ is isotropic,}$$

[1] The transfer matrix is called *lead field basis* in [37]

has to be assumed to allow for the use of the fast transfer matrix approach because the entries of the matrices K^{corr} and S in equations (10), (11) depend on the conductivity at the dipole position. In contrast, the conductivity for different source positions might vary for the presented full subtraction approach. This is a further advantage of the full subtraction approach, since the cortex is sometimes referred to be a slightly anisotropic conductor (see the discussion section).

5 Influence Matrix

Most inverse EEG and MEG source analysis algorithms are based on precomputed forward solutions for a set of anatomically and physiologically meaningful sources, i.e., right-hand sides $(f^y)_{y \in Y}$. It is then advantageous to precompute the so-called *influence matrix*

$$L \in \mathbb{R}^{m \times \#Y},$$

whose entry $L_{i,y}$ is the forward computed field for source y at sensor i. The influence matrix can be computed by

(1) multiplying each right-hand side b^y with the transfer matrix B in $\mathcal{O}(mN\#Y)$ and each analytic solution $u^{\infty,y}$ by $\hat{A}$, or
(2) multiplying each row of the transfer matrix B (from the left) by the matrix

$$R \in \mathbb{R}^{N \times \#Y}, \qquad R_{i,y} := b_i^y$$

of right-hand sides (and adding the term $\hat{A}u^{\infty,y}$). The complexity for the naive approach would again be $\mathcal{O}(mN\#Y)$. However, the matrix R can be cast into the $\mathcal{H}$-matrix format [37] so that each matrix-vector multiplication is of complexity $\mathcal{O}(N \log N)$. The multiplication $\hat{A}u^{\infty,y}$ can as well be performed after casting the right-hand sides $u^{\infty,y}$ into the $\mathcal{H}$-matrix format. Hence, the total complexity reduces in this case to

$$\mathcal{O}(mN \log N).$$

6 Validation and numerical experiments

6.1 Analytical solution in an anisotropic multilayer sphere model

De Munck and Peters [6] derive series expansion formulas for a mathematical dipole in a multilayer sphere model, denoted here as the "analytical solution". A rough overview of the formulas will be given in this section. The model consists of S shells with radii $r_S < r_{S-1} < \ldots < r_1$ and constant radial, $\sigma^{\mathrm{rad}}(r) = \sigma_j^{\mathrm{rad}} \in \mathbb{R}^+$, and constant tangential conductivity, $\sigma^{\mathrm{tang}}(r) = \sigma_j^{\mathrm{tang}} \in \mathbb{R}^+$, within each layer $r_{j+1} < r < r_j$. It is assumed that the source at position x_0 with radial coordinate $r_0 \in \mathbb{R}$ is in a more interior layer than the measurement electrode at position $x_e \in \mathbb{R}^3$ with radial coordinate $r_e = r_1 \in \mathbb{R}$. The spherical harmonics expansion for the mathematical dipole (1) is expressed in terms of the gradient of the monopole potential to the source point. Using an asymptotic approximation and an addition-subtraction method to speed up the series convergence yields

$$\mathrm{u}_{\mathtt{ana}}(x_0, x_e) = \frac{1}{4\pi}\langle \mathbf{M}, S_0 \frac{x_e}{r_e} + (S_1 - \cos\omega_{0e} S_0)\frac{x_0}{r_0}\rangle$$

with ω_{0e} being the angular distance between source and electrode, and with

$$\begin{aligned} S_0 = & \frac{F_0}{r_0}\frac{\Lambda}{(1 - 2\Lambda\cos\omega_{0e} + \Lambda^2)^{3/2}} \\ & + \frac{1}{r_0}\sum_{n=1}^{\infty}\left\{(2n+1)R_n(r_0, r_e) - F_0\Lambda^n\right\} P_n'(\cos\omega_{0e}) \end{aligned} \tag{12}$$

and

$$\begin{aligned} S_1 = & F_1\frac{\Lambda\cos\omega_{0e} - \Lambda^2}{(1 - 2\Lambda\cos\omega_{0e} + \Lambda^2)^{3/2}} \\ & + \sum_{n=1}^{\infty}\left\{(2n+1)R_n'(r_0, r_e) - F_1 n\Lambda^n\right\} P_n(\cos\omega_{0e}). \end{aligned} \tag{13}$$

The coefficients R_n and their derivatives, R_n', are computed analytically and the derivative of the Legendre polynomials, P_n, are determined by means of a recursion formula. We refer to [6] for the derivation of the above series of differences [2] and for the definition of F_0, F_1 and Λ. Here, it is only important

[2] The following is a result of a discussion with J.C. de Munck: While constants in formulas (71) and (72) in the original paper [6] have to be flipped, our versions of S_0 and S_1 in Equations (12) and (13) are correct.

that the latter terms are independent of n and that they can be computed from the given radii and conductivities of layers between source and electrode and of the radial coordinate of the source. The computations of the series (12) and (13) are stopped after the k-th term, if the following criterion is fulfilled

$$\frac{t_k}{t_0} \leq \upsilon, \qquad t_k := (2k+1)R'_k - F_1 k \Lambda^k. \tag{14}$$

In the following simulations, a value of 10^{-6} is chosen for υ in (14). Using the asymptotic expansion, no more than 30 terms are needed for the series computation at each electrode.

6.2 Numerical quadrature and FE solver

Table 1
Quadrature formulas of Stroud [28] for the volume integral from Equation (7) and the surface integral from Equation (8) .

Formula	degree	number integration points	Reference
Volume integral from Equation (7)			
$T_n : 1-1$	1	1	[28, Chapter 8.8, p.307]
$T_n : 2-1$	2	$n+1$	[28, Chapter 8.8, p.307]
$T_3 : 7-1$	7	64	[28, Chapter 8.8, p.315]
Surface integral from Equation (8)			
$T_n : 1-1$	1	1	[28, Chapter 8.8, p.307]
$T_n : 2-1$	2	$n+1$	[28, Chapter 8.8, p.307]
$T_2 : 7-1$	7	16	[28, Chapter 8.8, p.314]

For the numerical integration of the right-hand side (7), (8), we use quadrature formulas of Stroud [28]. As shown in Table 1, the overall numerical accuracy of the full subtraction approach will be evaluated for quadrature orders of 1, 2 and 7. Our notation in Table 1 closely follows the one of the tables in [28]. T_n indicates an n-dimensional simplex [28, Chapter 7.8] (in our case: $n = 3$).

We employ an algebraic multigrid preconditioned conjugate gradient (AMG-CG) method for solving the linear system (6). We solve up to a relative error of 10^{-8} in the controllable $KN^{-1}K$-energy norm (with N^{-1} being one V-cycle of the AMG) [34,9].

6.3 Error criteria

We compare numerical solutions with analytical solutions using three error criteria that are commonly evaluated in source analysis [14,3,29,13,23,33]. The *relative (Euclidean) error* (RE) is defined as

$$\mathrm{RE} = ||\underline{u}^{\mathtt{num}} - \underline{u}^{\mathtt{ana}}||_2 / ||\underline{u}^{\mathtt{ana}}||_2,$$

where $\underline{u}^{\mathtt{ana}}, \underline{u}^{\mathtt{num}} \in \mathbb{R}^{\mathrm{m}}$ denote the analytical and the numerical solution vector, resp., at m measurement electrodes. In order to better distinguish between the topography (driven primarily by changes in dipole location and orientation) and the magnitude error (indicating changes in source strength), Meijs et al. [14] introduced the *relative difference measure* (RDM)

$$\mathrm{RDM} = \sqrt{\sum_{i=1}^{\mathrm{m}} \left(\underline{u}_i^{\mathtt{ana}} / ||\underline{u}^{\mathtt{ana}}||_2 - \underline{u}_i^{\mathtt{num}} / ||\underline{u}^{\mathtt{num}}||_2\right)^2}$$

(for zero-mean data holds $0 \leq \mathrm{RDM} \leq 2$ [23]) and the *magnification factor* (MAG)

$$\mathrm{MAG} = ||\underline{u}^{\mathtt{num}}||_2 / ||\underline{u}^{\mathtt{ana}}||_2$$

(minimal error: MAG = 1), respectively.

6.4 Validation platform

Table 2
Parameterisation of the anisotropic four layer sphere model.

Medium	Scalp	Skull	CSF	Brain
Outer shell radius	92mm	86mm	80mm	78mm
Tangential conductivity	0.33S/m	0.042S/m	1.79S/m	0.33S/m
Radial conductivity	0.33S/m	0.0042S/m	1.79S/m	0.33S/m

The validation of the presented full subtraction approach is carried out in a four compartment sphere model with anisotropic skull compartment, whose parameterisation is shown in Table 2. For the choice of these parameters, we closely followed [11,13].

The numerical forward solution is validated by means of the corresponding analytic solution for dipoles located on the y axis at depths of 0% to 98.7%

(in 1mm steps) of the brain compartment (78mm radius) using both radial and tangential dipole orientations. *Eccentricity* is defined here as the percent ratio of the distance between the source location and the model midpoint divided by the radius of the inner sphere (78mm radius). The most eccentric source considered is thus only 1mm below the CSF compartment. Tangential sources are oriented in the +z axis and radial dipoles in the +y axis. The dipole amplitudes are chosen to be 1nAm.

To achieve error measures which are independent of the specific choice of the sensor configuration, we distribute electrodes in a most-regular way over a given sphere surface. In this way we generate a 748 electrode configuration on the surface of the outer sphere.

6.5 Tetrahedral mesh generation.

The FE meshes of the four layer sphere model are generated by the software TetGen [25] which uses a *Constrained Delaunay Tetrahedralisation* (CDT) approach [27]. The meshing procedure starts with the preparation of a suitable boundary discretisation of the model. To begin with, for each of the four layers and for a given triangle edge length, nodes are distributed in a most-regular way and connected through triangles. This yields a valid triangular surface mesh for each of the four layers. Meshes of different layers are not intersecting each other. The CDT approach is then used to construct a tetrahedralisation conforming to the surface meshes. It first builds a Delaunay tetrahedralisation of the vertices of the surface meshes. It then uses a local degeneracy removal algorithm combining vertex perturbation and vertex insertion to construct a new set of vertices which includes the input set of vertices. In the last step, a fast facet recovery algorithm is used to construct the CDT [27].

This approach is combined with two further constraints to the size and shape of the tetrahedra. The first constraint can be used to restrict the volume of the generated tetrahedra in a certain compartment, the so-called *volume constraint*. The second constraint is important for the generation of quality tetrahedra. If R denotes the radius of the unique circumsphere of a tetrahedron and L its shortest edge length, the so-called *radius-edge ratio* of the tetrahedron can be defined as

$$Q = \frac{R}{L}.$$

The radius-edge ratio can distinguish almost all badly-shaped tetrahedra except one type of tetrahedra, so-called *slivers*. A sliver is a very flat tetrahedron which has no small edges, but can have arbitrarily large dihedral angles (close

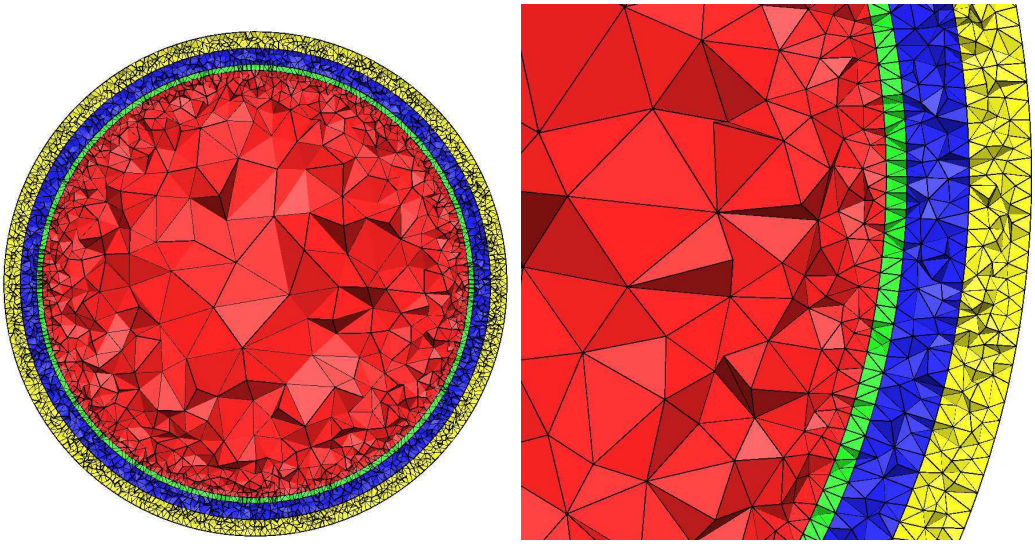

Fig. 1. Cross-section of the tetrahedral mesh `tet360K` of the four compartment sphere model. Visualisation is done using Tetview [26].

to π). For this reason, an additional mesh smoothing and optimization step is used to remove the slivers and improve the overall mesh quality.

Table 3
The number of nodes and elements of the three tetrahedra models used for numerical accuracy tests.

Model	Nodes	Elements
tet360K	360,056	2,165,281
tet287K	287,217	1,712,360
tet39K	38,928	229,311

In Table 3, the number of nodes and elements of the three tetrahedral meshes are shown which will be used for numerical accuracy tests. The tetrahedral mesh `tet360K` of the four compartment sphere model is shown in Figure 1. For this model, we distribute 31,680 nodes on each of the four surfaces for the CDT procedure. We allow for a maximal radius-edge ratio of $Q = 1.2$. The volumes of the tetrahedra in the compartments skin, skull and CSF are furthermore restricted correspondingly to the chosen surface triangle edge length. As it can be observed in Figure 1, no volume constraint is used for the brain layer since for this compartment, the entries of the volume integral (7) are zero ($(\sigma(y) - \sigma(x)) = 0$ for all x in the brain compartment) so that a coarse resolution will not spoil the overall numerical accuracy, but reduce the computational amount of work.

6.6 *Validation results in anisotropic four layer sphere model*

6.6.1 *Evaluation with regard to right-hand side quadrature order*

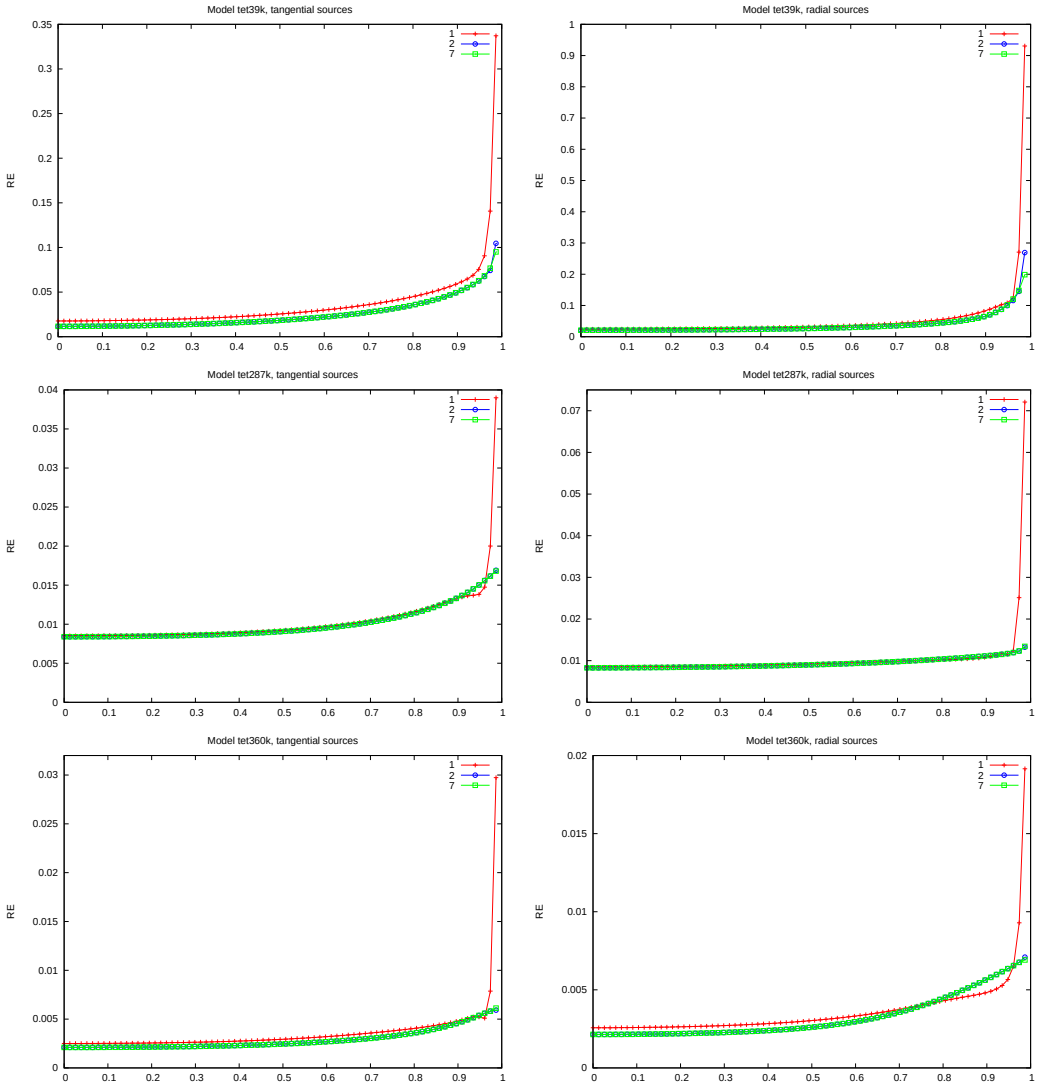

Fig. 2. Relative error for tangentially (left) and radially (right) oriented dipoles with quadrature orders of 1,2 and 7: Model `tet39K` (top row), `tet287K` (middle row) and `tet360K` (bottom row). Note the different scaling for the RE.

In the first study, we compare the numerical accuracy of the presented full subtraction approach for quadrature formulas with different integration order for the right-hand side (7), (8). The goal of this study is to verify that second order integration formulas are necessary and sufficient as stated in Remark 11. Figure 2 shows the relative errors between the numerical and the quasi-analytical solutions for tangential (left column) and radial sources (right column) for the models `tet39K` (top row), `tet287K` (middle row) and `tet360K` (bottom row) from Table 3. The different quadrature orders of 1, 2 and 7 are

represented with different labels in the figure. Especially for eccentric sources, the integration order 1 performs worse than order 2. This shows the necessity of second order integration. Second order integration is also sufficient since the difference between order 2 and 7 in Figure 2 is not visible (models `tet287K` and `tet360K`) or very small (model `tet39K`) and, in any case, not worth the much larger computational amount of work for the higher quadrature order.

6.6.2 Evaluation with regard to mesh resolution

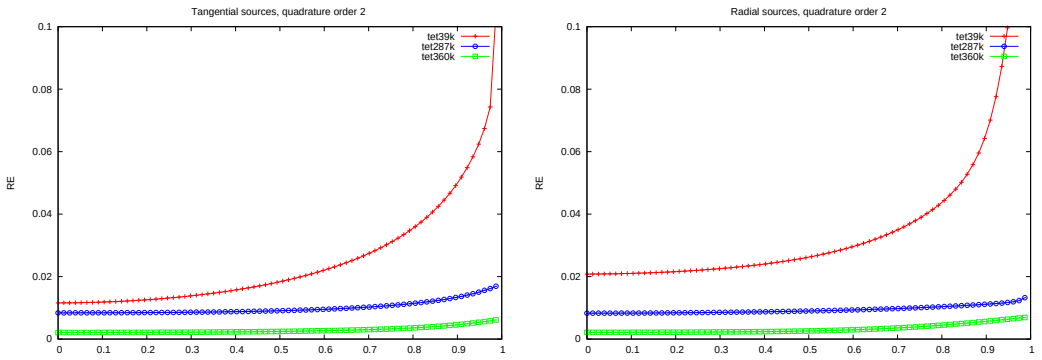

Fig. 3. Relative error for the FE meshes of Table 3 and quadrature order 2 for tangentially (left) and radially oriented dipoles (right).

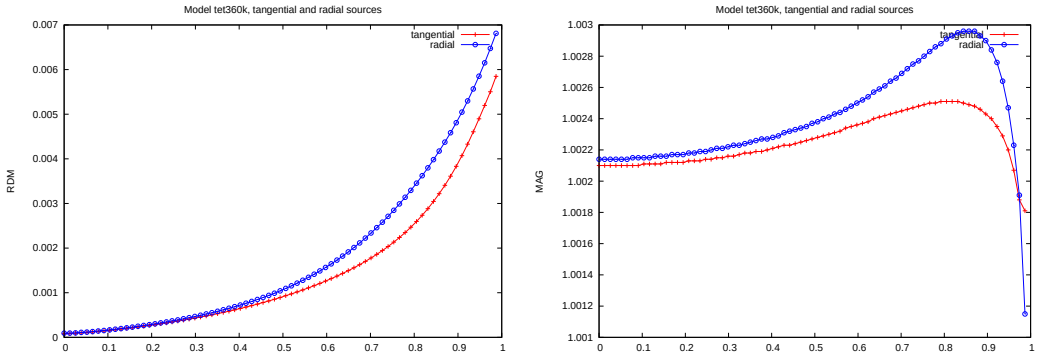

Fig. 4. RDM (left) and MAG errors (right) for model `tet360K` for tangentially and radially oriented dipoles.

In the second study, we evaluate the numerical errors with regard to the resolution of the FE discretisation. Following the results of Section 6.6.1, a quadrature order of 2 is used for the integration of the right-hand side. Figure 3 shows the RE for the three models of Table 3 for tangentially (left) and radially oriented dipoles (right). A clear convergence can be observed, i.e., the RE decreases over all eccentricities with increasing mesh resolution. The accuracy increase is especially distinct for eccentric sources. With the finest model `tet360K`, we are able to decrease the maximal RE over all eccentricities and source orientations to a value of 0.71% for the most eccentric radial source 1mm below the CSF compartment. Figure 4 shows the corresponding RDM

and MAG errors for the finest model `tet360K`. The largest topography error is an RDM of 0.34% and the largest magnitude error a MAG of 0.3%.

6.6.3 Comparison of projected and full subtraction approach

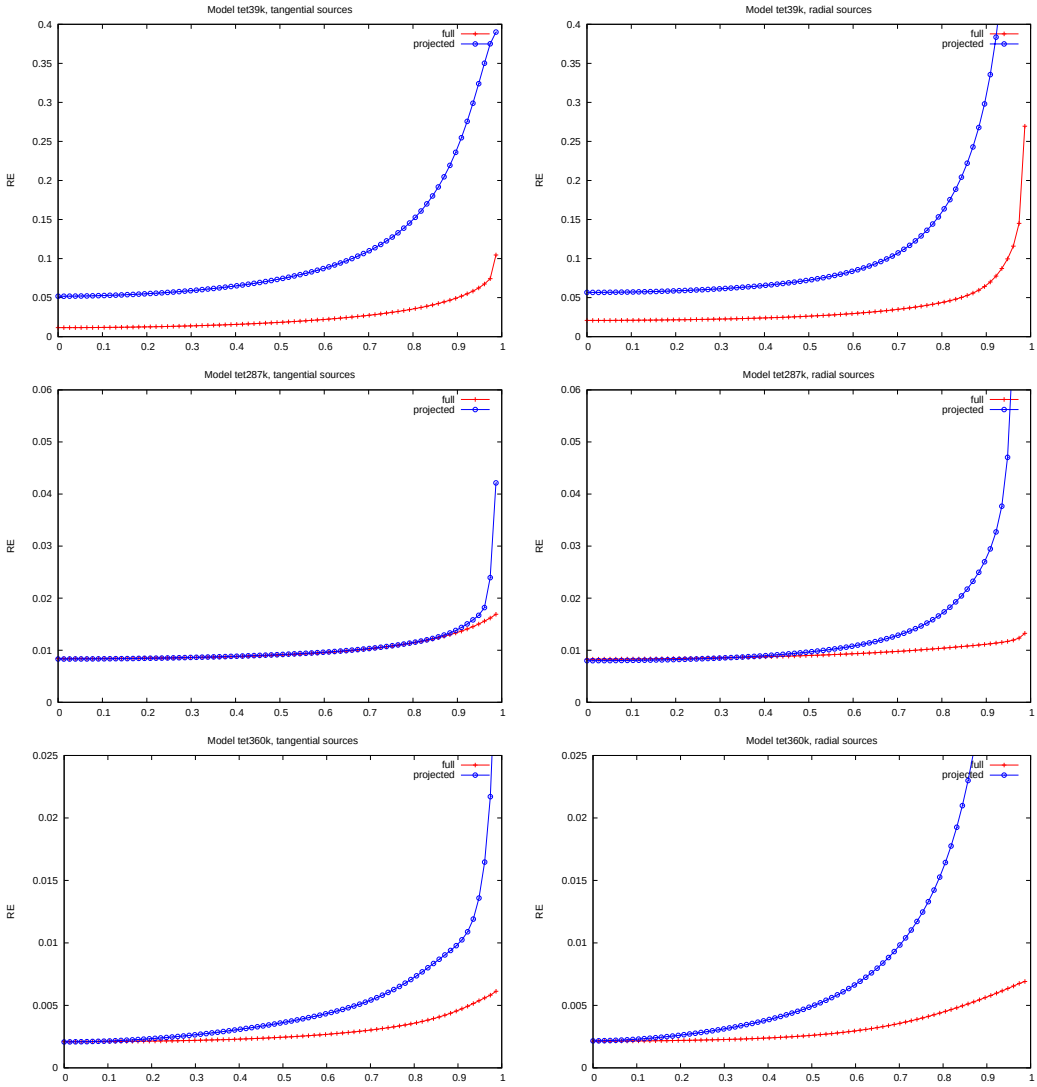

Fig. 5. Comparison between the presented full subtraction approach and the projected subtraction approach from [33] with regard to the relative error for tangential (left) and radial sources (right): Model `tet39K` (top row), `tet287K` (middle row) and `tet360K` (bottom row).

In a last study, we compare the presented full subtraction approach with the projected subtraction method from [33]. Figure 5 shows the RE for tangential (left column) and radial sources (right column) for the models `tet39K` (top row), `tet287K` (middle row) and `tet360K` (bottom row) from Table 3. It can be summarized that the presented full subtraction approach is a major step forward with regard to accuracy for all examined mesh resolutions, which

is especially prominent for eccentric sources. For the finest model `tet360K` (bottom row), the largest RE of 5% for the projected subtraction approach is reduced by more than a factor of 7 to a maximal RE of 0.71% for the presented full subtraction approach.

7 Discussion and conclusion

We present theory and numerical experiments of a full subtraction approach to model a mathematical dipole in finite element (FE) method based electroencephalography (EEG) source reconstruction. Since the magnetoencephalography (MEG) forward problem is also based on the computed electric potential (see, e.g., [37]), our method is directly applicable to MEG source analysis. We embed the approach for the computation of the correction potential in the general FE convergence theory and find that under the assumption of higher regularity than H^1, i.e., $H^{1+\varepsilon}(\Omega)$ with $\varepsilon \in]0,1[$, it might be important to integrate the right-hand side of the differential equation for the correction potential with a quadrature order of 2 for achieving highest possible accuracy.

We validate our implementation of the method in a four-compartment sphere model with anisotropic skull layer. In the numerical experiments, we find that second order integration is necessary and sufficient, as the theory predicts. The evaluation of the convergence order is a difficult task because the convergence constant is strongly depending on the distance of the source to the next conductivity discontinuity (a theoretical reasoning for this fact is given in [33]). Furthermore, our quasi-analytical formulas are currently limited to measurement points with larger radial location components than the source. Consequently, error-norms of the entire numerical potential solution could not yet be computed. However, with regard to the EEG inverse problem, an evaluation of the numerical accuracy at the surface electrodes seems to be sufficient. Our new approach is shown to converge, i.e., with increasing mesh size, numerical errors decrease. We consider it to be very progressive that the full subtraction method yields a maximal relative error (RE) of 0.71% over all source eccentricities for sources up to 1mm below the CSF compartment for the finest of the examined high-quality constrained Delaunay tetrahedralisation (CDT) FE meshes with 360K nodes which is not locally refined around the source singularity: maximal examined eccentricity of 98.7%, maximal relative difference measure (maxRDM): 0.34%, maximal magnification factor (maxMAG): 0.3%. Schimpf et al. [23] investigate an FE subtraction approach in a four layer sphere model with isotropic skull and sources up to 1mm below the CSF compartment. In their article, a regular 1mm cube model is used (thus a much higher FE resolution) and a maxRDM of 7% and a maxMAG of 25% is achieved. In a locally refined (around the source singularity) tetrahedral mesh with 12,500 nodes of a four layer sphere model with anisotropic

skull and first order FE basis functions, Bertrand et al. [3] report numerical accuracies up to a maximal eccentricity of 97.6%. A maximal RDM of above 20% and a maximal MAG up to 70% are documented for the most eccentric source. Van den Broek [29] also uses a locally refined (around the source singularity) tetrahedral mesh with 3,073 nodes of a three layer sphere model with anisotropic skull. For the maximal examined eccentricity of 94.2%, an RDM of up to 50% is given. It is mentioned in the conclusion that in some cases the accuracy can not further be improved by adding points globally as the numerical stability of the matrix equation that is to be solved is reduced. Marin et al. [13] use second order FE basis functions, but their finest tetrahedral mesh of 87,907 nodes is restricted to eccentricities of 81% in order to reach a sufficient accuracy for radial dipole forward solutions in a three compartment sphere model with anisotropic skull. Awada et al. [1] implement a 2D subtraction approach and compare its numerical accuracy with a direct potential method in a 2D sphere model. A direct comparison with our results is therefore difficult, but the authors conclude that the subtraction method is generally more accurate than the direct approach. In a direct comparison with the projected subtraction approach from [33], we find that the new method is by an order of magnitude more accurate for dipole sources close to the next conductivity discontinuity. The fact that, in a realistic head model, most sources of interest have eccentricities between 50% and 98% shows the importance of our results.

Besides its higher accuracy, the possibility of also modelling cortical anisotropy in combination with the efficient transfer matrix approach might be a further advantage of the full subtraction approach when compared to the projected subtraction approach from [33], since the cortex is sometimes referred to be a slightly anisotropic conductor [39,19]. There is a strong debate about cortical anisotropy since DTI measurements rather show that the grey matter is an isotropic compartment [24]. However, at least the infant grey matter might be slightly anisotropic because of yet less developed synaptic connections to the cortical pyramidal cells. Furthermore, it is shown that even slight degrees of cortical anisotropy might already have a large influence on the forward EEG and MEG modelling accuracy [12,36]. In subsequent studies, we will perform profound comparisons of the full subtraction approach with direct potential methods in locally and remotely anisotropic volume conductors.

8 Acknowledgement

This work was supported by the Deutsche Forschungsgemeinschaft (WO1425/1-1, GR3179/1-1). The authors would like to thank J.C. de Munck for providing the software for the quasi-analytical solution in multilayer sphere models and for his quick responses whenever needed.

References

[1] K. Awada, D. Jackson, J. Williams, D. Wilton, S. Baumann, A. Papanicolaou, Computational aspects of finite element modeling in EEG source localization, IEEE Trans Biomed. Eng. 44 (8) (1997) 736–751.

[2] S. Baumann, D. Wozny, S. Kelly, F. Meno, The electrical conductivity of human cerebrospinal fluid at body temperature, IEEE Trans Biomed. Eng. 44 (3) (1997) 220–223.

[3] O. Bertrand, M. Thévenet, F. Perrin, 3D finite element method in brain electrical activity studies, in: J. Nenonen, H. Rajala, T. Katila (eds.), Biomagnetic Localization and 3D Modelling, Report of the Dep. of Tech.Physics, Helsinki University of Technology, 1991.

[4] D. Braess, Finite Elements: Theory, Fast Solvers and Applications in Solid Mechanics., Cambridge University Press, 2007.

[5] H. Buchner, G. Knoll, M. Fuchs, A. Rienäcker, R. Beckmann, M. Wagner, J. Silny, J. Pesch, Inverse localization of electric dipole current sources in finite element models of the human head, Electroenc. Clin. Neurophysiol. 102 (1997) 267–278.

[6] J. de Munck, M. Peters, A fast method to compute the potential in the multi sphere model, IEEE Trans Biomed. Eng. 40 (11) (1993) 1166–1174.

[7] J. de Munck, B. van Dijk, H. Spekreijse, Mathematical dipoles are adequate to describe realistic generators of human brain activity, IEEE Trans Biomed. Eng. 35 (11) (1988) 960–966.

[8] M. Fuchs, M. Wagner, H. Wischmann, T. Köhler, A. Theißen, R. Drenckhahn, H. Buchner, Improving source reconstructions by combining bioelectric and biomagnetic data, Electroenc. Clin. Neurophysiol. 107 (1998) 93–111.

[9] G. Haase, M. Kuhn, S. Reitzinger, Parallel AMG on distributed memory computers, SIAM J. Sci.Comp. 24 (2) (2002) 410–427.

[10] W. Hackbusch, Iterative solution of large sparse systems of equations, Springer Verlag, Applied Mathematical Sciences 95, 1994.

[11] H. Hallez, B. Vanrumste, P. V. Hese, Y. D'Asseler, I. Lemahieu, R. V. de Walle, A finite difference method with reciprocity used to incorporate anisotropy in electroencephalogram dipole source localization., Phys.Med.Biol. 50 (2005) 3787–3806.

[12] J. Haueisen, C. Ramon, H. Brauer, H. Nowak, The influence of local conductivity changes on MEG and EEG, Biomedizinische Technik 45 (7-8) (2000) 211–214.

[13] G. Marin, C. Guerin, S. Baillet, L. Garnero, M. G., Influence of skull anisotropy for the forward and inverse problem in EEG: simulation studies using the FEM on realistic head models, Human Brain Mapping 6 (1998) 250–269.

[14] J. Meijs, O. Weier, M. Peters, A. van Oosterom, On the numerical accuracy of the boundary element method, IEEE Trans Biomed. Eng. 36 (1989) 1038–1049.

[15] C. Michel, M. Murray, G.Lantz, S.Gonzalez, L.Spinelli, R. de Peralta, EEG source imaging, Clin.Neurophysiol. 115 (2004) 2195–2222, invited review.

[16] M. Mohr, Simulation of Bioelectric Fields: The Forward and Inverse Problem of Electroencephalographic Source Analysis, vol. Band 37 of Arbeitsberichte des Instituts für Informatik, Friedrich-Alexander-Universität Erlangen-Nürnberg, 2004, iSSN 1611-4205.

[17] S. Murakami, Y. Okada, Contributions of principal neocortical neurons to magnetoencephalography and electroencephalography signals, J.Physiol. 575 (3) (2006) 925–936.

[18] C. Pantev, M. Hoke, B. Lütkenhöner, K. Lehnertz, Tonotopic organization of the auditory cortex: Pitch versus frequency representation, Science 246 (1989) 486–488.

[19] M. Peters, J. de Munck, The influence of model parameters on the inverse solution based on MEGs and EEGs, Acta Otolaryngol [Suppl] (Stockh) 491 (1991) 61–69.

[20] R. Plonsey, D. Heppner, Considerations on quasi-stationarity in electrophysiological systems, Bull.math.Biophys. 29 (1967) 657–664.

[21] C. Ramon, P. Schimpf, J. Haueisen, M. Holmes, A. Ishimaru, Role of soft bone, CSF and gray matter in EEG simulations, Brain Topography 16 (4) (2004) 245–248.

[22] J. Sarvas, Basic mathematical and electromagnetic concepts of the biomagnetic inverse problem, Phys.Med.Biol. 32 (1) (1987) 11–22.

[23] P. Schimpf, C. Ramon, J. Haueisen, Dipole models for the EEG and MEG, IEEE Trans Biomed. Eng. 49 (5) (2002) 409–418.

[24] J. S. Shimony, R. McKinstry, E.Akbudak, J.A.Aronovitz, A.Z.Snyder, N.F.Lori, T.S.Cull, T.E.Conturo, Quantitative diffusion-tensor anisotropy brain MR imaging: Normative human data and anatomic analysis, Radiology 212 (1999) 770–784.

[25] H. Si, Tetgen, Tech. rep., Weierstrass Institute for Applied Analysis and Stochastics, http://tetgen.berlios.de (2007).

[26] H. Si, Tetview, Tech. rep., Weierstrass Institute for Applied Analysis and Stochastics, http://tetgen.berlios.de/tetview.html (2007).

[27] H. Si, K. Gärtner, Meshing piecewise linear complexes by constrained delaunay tetrahedralizations, September 2005, proceedings of the 14th Int.Meshing Roundtable.

[28] A. H. Stroud, Approximate calculation of multiple integrals, Prentice-Hall, Inc., 1971.

[29] S. van den Broek, Volume conduction effects in EEG and MEG, Ph.D. thesis, Proefschrift Universiteit Twente Enschede, The Netherlands (1997).

[30] T. Waberski, H. Buchner, K. Lehnertz, A. Hufnagel, M. Fuchs, R. Beckmann, A. Rienäcker, The properties of source localization of epileptiform activity using advanced headmodelling and source reconstruction, Brain Top. 10 (4) (1998) 283–290.

[31] C. Wolters, A. Anwander, D.Weinstein, M.Koch, X.Tricoche, R.S.MacLeod, Influence of tissue conductivity anisotropy on EEG/MEG field and return current computation in a realistic head model: A simulation and visualization study using high-resolution finite element modeling., NeuroImage 30 (3) (2006) 813–826, http://dx.doi.org/10.1016/j.neuroimage.2005.10.014.

[32] C. Wolters, J. de Munck, Volume conduction, Encyclopedia of Computational Neuroscience, Scholarpedia, invited review, http://www.scholarpedia.org.

[33] C. Wolters, H. Köstler, C. Möller, J. Härtlein, L. Grasedyck, W. Hackbusch, Numerical mathematics of the subtraction method for the modeling of a current dipole in EEG source reconstruction using finite element head models., SIAM J. on Scientific ComputingIn press.

[34] C. Wolters, M. Kuhn, A. Anwander, S. Reitzinger, A parallel algebraic multigrid solver for finite element method based source localization in the human brain, Comp.Vis.Sci. 5 (3) (2002) 165–177.

[35] C. H. Wolters, A. Anwander, G. Berti, U. Hartmann, Geometry-adapted hexahedral meshes improve accuracy of finite element method based EEG source analysis., IEEE Trans.Biomed.Eng. 54 (8) (2007) 1446–1453.

[36] C. H. Wolters, A. Anwander, X. Tricoche, S. Lew, C. Johnson, Influence of local and remote white matter conductivity anisotropy for a thalamic source on EEG/MEG field and return current computation, Int.Journal of Bioelectromagnetism 7 (1) (2005) 203–206.

[37] C. H. Wolters, L. Grasedyck, W. Hackbusch, Efficient computation of lead field bases and influence matrix for the FEM-based EEG and MEG inverse problem, Inverse Problems 20 (4) (2004) 1099–1116.

[38] Y. Yan, P. Nunez, R. Hart, Finite-element model of the human head: Scalp potentials due to dipole sources, Med.Biol.Eng.Comput. 29 (1991) 475–481.

[39] M. Yedlin, H. Kwan, J. Murphy, H. Nguyen-Huu, J. Wong, Electrical conductivity in cat cerebellar cortex, Exp.Neurol. 43 (1974) 555–569.